



## Magnetohydrodynamic (MHD) Flow in a Channel Including a Rotating Cylinder

F. Mobadersani\*, S. Bahjat

Department of Renewable Energy, Faculty of Mechanical Engineering, Urmia University of Technology, Urmia, Iran

### PAPER INFO

#### Paper history:

Received 02 July 2019

Received in revised form 16 October 2020

Accepted 29 October 2020

#### Keywords:

Nanofluid

Heat Transfer

Magnetohydrodynamics

Finite Element

Rotational Cylinder

### ABSTRACT

Heat transfer analysis in channels and enclosures has significant attention nowadays. In the present work, fluid flow and heat transfer of a vertical channel consisting of a rotating cylinder utilizing nanofluid have been studied, numerically. Uniform magnetic field has been applied to the fluid field. Different cylinder rotation directions, Hartmann number and rotational velocity of cylinder configurations have been considered. The results indicate that by increasing the Hartmann number, for low values of non-dimensional angular velocity the average Nusselt number increases. In addition, in higher Hartmann numbers, the average Nusselt number does not change remarkably with non-dimensional angular velocity. Furthermore, studying lift and drag coefficients demonstrate that in a constant Hartmann number, the highest drag coefficient takes place in maximum cylinder angular velocity. Additionally, almost uniform distribution of drag coefficient can be seen in higher Hartmann numbers. The numerical results have been compared with the previously reported results. This comparison illustrates excellent agreement between them.

doi: 10.5829/ije.2021.34.01a.25

## 1. INTRODUCTION

Poor thermal characteristics of working fluids such as water, ethylene glycol, and oil are the main obstacle of the convectional heat transfer. In order to assess high thermal conductivity, the idea of adding metallic and non-metallic particles to common fluids was already existed. Because of the low development of technology in the past, they added coarse particles with average diameters of the millimeter and micrometer to base fluids to improve their thermal characteristics. Adding coarse particles to the convectional fluids causes to increase pressure drop, gravitic sedimentation, clog the entrance of channels and pipes and erosion of the walls. One of the innovative ways to overcome these problems is adding the metallic – nonmetallic nanoscale particles to the base fluids and make nanofluids. Nanofluids are combinations of nanoparticles with a maximum volume fraction of 5% added to the base fluids. Additionally, the average diameters of those particles are lesser than 100nm. Furthermore, the general types of nanoparticles which used in nanofluids are oxides of metallic and metallic

particles such as alumina, Cu, CuO, magnetite and organic particles such as carbon nanotubes. In addition to high stability of nano size particles in base fluid, using nanofluids leads to increase thermal conductivity of fluid significantly [1-6]. Many researchers have investigated the influences of adding those particles on applications such as drug targeting, heat exchangers, power plants and etc. Gravndyan et al. [7] have investigated the effects of ribs mounted on channel surface utilizing Ti<sub>2</sub>O/water nanofluid. They reported in all values of Reynolds number and ribs aspects ratios, increasing volume fraction of nanoparticle raise the average Nusselt number. In another study, Ahmadi et al. [8] reported, despite pressure drop increases, augmenting nanoparticles volume concentration has positive impacts on thermal conductivity. Thermal conductivity increase with temperature increment is reported in Bahiraei and Mashaei investigation [9]. They reported that by utilizing small nanoparticle, effects of temperature on thermal conductivity increase. Ho et al. [10] experimentally investigated the effects of nanoparticle volume fraction on heat transfer efficiency in a microchannel. The results

\*Corresponding Author Institutional Email:  
f.mobadersani@mee.uut.ac.ir (F. Mobadersani)

indicate that in a special Reynolds number by raising nanoparticle volume fraction, the average Nusselt number enhances. In addition, they obtained 53% increment in average Nusselt at  $Re=1641$  and volume fraction of 1% in comparison with the pure water. Additionally, Heydari and Kermani [11] studied effects of blocks attached to the bottom wall of the channel utilizing nanofluid. Their results show that in all values of Reynolds number and volume fractions of nanoparticles, augmenting numbers of blocks enhances top wall average Nusselt number. Khanafer et al. [12] presented a numerical simulation of nanofluid inside a cavity for various Grashof numbers. They reported increases in volume fraction of nanoparticles at any Grashof number enhances the average Nusselt number, although intensity of increasing is severe in higher Grashof numbers. Santra et al. [13] studied the influences of Reynolds number and volume fraction of nanoparticles on the flow and heat transfer in two parallel plates utilizing nanofluid as Newtonian and non-Newtonian fluid. Their results show that the enhancement of the average Nusselt number due to increasing volume fraction in consideration of non-Newtonian fluid is higher than Newtonian fluid. Roslan et al. [14] numerically investigated square enclosure with a inner rotating cylinder utilizing different types of the nanoparticles. They reported Ag particles shows better efficiency in convection heat transfer with comparison to  $Ti_2O$ , Cu and  $Al_2O_3$ . In addition, their results illustrate cylinder rotation in any direction in case of  $R=0.2$ , (dimensionless radius of the cylinder) has negative impacts on the average Nusselt number.

Hydrodynamical study of electrical conductive liquids under the influence of magnetic field is called Magneto-hydrodynamics. In the other word, MHD is the investigation of the flow-structure by applying a uniform magnetic field and considering effects of Lorentz force. Lorentz force is the magnetic force which rises from the electrical conductivity of fluids and acts as a braking force. MHD flows has a wide range of industrial applications such as crystal growth, metal casting, polymer industry, and liquid metal cooling blankets for fusion reactors [15-19]. Aminossadati et al. [20] reported by applying a uniform magnetic field, horizontal velocity profile along centerline of the channel decrease whereas at the vicinity of the walls increase. As well as, they indicated that raising Hartmann number augments the convective heat transfer. Heydari et al. [21] numerically investigated the effects of nanoparticles concentration and effects of Lorentz force in the horizontal channel. Their results demonstrate that exerting magnetic field leads to reduce temperature layer thickness and consequently accelerate heat removal from the surface. Additionally, they reported raising nanoparticles volume fraction enhances the temperature layer thickness. Selimefendigil and Oztop [22] studied numerically

mixed convection lid-driven enclosure with a inner rotating cylinder. Their results show that existing magnetic field has negative impacts on convective heat transfer. Furthermore, augmenting Richardson number results in average Nusselt number enhancement. Hosseini et al. [23] reported, the uniform magnetic field affects the velocity profile and forces it to be uniform. On the other hand, the magnetic field increases velocity gradient near the walls which results in convective heat transfer improvement. Oztop et al. [24] numerically investigated the effects of Grashof and Hartmann numbers in lid-driven cavity. Their results indicate that at any Grashof number, the existence of a magnetic field causes convective heat transfer decrement. Aminfar et al. [25] numerically investigated the effects of magnetic fields in straight duct utilizing ferrofluid by considering both FHD and MHD approach. They concluded that by increasing the strength of Lorentz force, the velocity profile becomes flat and velocity gradient near the walls enhances. Consequently, the Nusselt number and friction coefficient rise due to increasing the strength of Lorentz force. Ma et al. [26] investigated flow in channel with the extended surface under the influence of a uniform magnetic field utilizing hybrid nanoparticles. They observed that Lorentz force strongly affects the structure of flow and weaken the strength of the recirculation zones. Besides, augmenting the magnetic field results in better convection heat transfer. Mahmoudi et al. [27] concluded that applying a uniform magnetic field leads to reduction in convection heat transfer. Additionally, in all values of Hartmann and Rayleigh numbers, by raising volume fraction of nanoparticles the average Nusselt number enhances.

To the best of our knowledge, there is no prior study on the MHD flow in the vertical channel with an inner rotating cylinder utilizing nanofluid. The goal of our study is to investigate the effects of magnetic field and cylinder rotation on convective heat transfer.

## 2. MATHEMATICAL FORMULATION

Schematic view of the study domain is represented in Figure 1. Consider two parallel vertical plates with wide  $H$  and length  $L=3.5H$  that Cu- $H_2O$  nanofluid flows through it. A rotating cylinder has been considered between the plates. The left wall of the channel is assumed to be adiabatic, while the right wall maintained at constant higher temperature  $T_h$ . No-slip boundary conditions are imposed on the left and right walls. Nanofluid with temperature of  $T_{in}$  ( $T_h > T_{in}$ ) and velocity,  $V_{in}$ , flows through the domain. An adiabatic cylinder with a diameter of  $d=0.4H$  is placed in the channel with the coordinance  $(0.5H, 0.5L)$  and rotates at constant angular velocity  $\omega$ . Uniform horizontal magnetic field applies to the channel. In addition, the gravitational

acceleration acts in the opposite y-direction. The geometry is assumed to be long enough to ignore end effects at the z-direction and can be considered as 2D dimensions. Ultrafine nanoparticles are assumed to have uniform shape and size. In addition, fluid phase and nanoparticles are assumed to be in thermal equilibrium with no-slip velocity between them. Thermophysical properties of the water and nanoparticles are taken to be constant except for density which changes linearly with Boussinesq approximation. The thermophysical properties of water and nanoparticles are shown in Table 1. According to the above assumptions, the continuity, momentum, and energy equations for the laminar, Newtonian fluid, incompressible and steady state flow by considering Boussinesq approximation with negligible viscous dissipation and Joule heating can be written as:

$$\frac{\partial u}{\partial x} + \frac{\partial v}{\partial y} = 0 \tag{1}$$

$$u \frac{\partial u}{\partial x} + v \frac{\partial u}{\partial y} = -\frac{1}{\rho_{nf}} \frac{\partial p}{\partial x} + \nu_{nf} \left( \frac{\partial^2 u}{\partial x^2} + \frac{\partial^2 u}{\partial y^2} \right) \tag{2}$$

$$u \frac{\partial v}{\partial x} + v \frac{\partial v}{\partial y} = -\frac{1}{\rho_{nf}} \frac{\partial p}{\partial y} + \nu_{nf} \left( \frac{\partial^2 v}{\partial x^2} + \frac{\partial^2 v}{\partial y^2} \right) - \frac{\sigma_{nf} B^2}{\rho_{nf}} v + \beta_{nf} g (T - T_{in}) \tag{3}$$

$$u \frac{\partial T}{\partial x} + v \frac{\partial T}{\partial y} = \alpha_{nf} \left( \frac{\partial^2 T}{\partial x^2} + \frac{\partial^2 T}{\partial y^2} \right) \tag{4}$$

Density and the specific heat capacity and the thermal expansion of the nanofluid are defined, respectively as [28-30]:

$$\rho_{nf} = (1 - \phi_p) \rho_{bf} + \phi_p \rho_p \tag{5}$$

$$(\rho c_p)_{nf} = (1 - \phi_p) (\rho c_p)_{bf} + \phi_p (\rho c_p)_p \tag{6}$$

$$(\rho \beta)_{nf} = (1 - \phi_p) (\rho \beta)_{bf} + \phi_p (\rho \beta)_p \tag{7}$$

where  $\phi$  is volume fraction of nanoparticles and the subscripts ‘bf’, ‘p’ and ‘nf’ denote the base fluid, nanoparticle and nanofluid, respectively. Furthermore, dynamic viscosity of the nanofluid according to the Brinkman [31] model is represented as:

$$\mu_{nf} = \frac{\mu_{bf}}{(1 - \phi)^{2.5}} \tag{8}$$

Thermal conductivity of the nanofluid by using uniform spherical shape of nanoparticles according to Wasp [32] can be expressed as:

$$\frac{k_{nf}}{k_{bf}} = \frac{k_p + 2k_{bf} - 2\phi_p (k_{bf} - k_p)}{k_p + 2k_{bf} + \phi_p (k_{bf} - k_p)} \tag{9}$$

Electrical conductivity of the nanofluid due to the Maxwell [33] model is:

$$\frac{\sigma_{nf}}{\sigma_{bf}} = 1 + \frac{3 \left( \frac{\sigma_p}{\sigma_{bf}} - 1 \right) \phi_p}{\left( \frac{\sigma_p}{\sigma_{bf}} + 2 \right) - \left( \frac{\sigma_p}{\sigma_{bf}} - 1 \right) \phi_p} \tag{10}$$

**2. 1. Non-dimensional Equations**

By defining non-dimensional parameters and substituting in the equations of (1-4), the dimensionless equations can be written as follows:

$$X = \frac{x}{2H}, Y = \frac{y}{2H}, U = \frac{u}{V_{in}}, V = \frac{v}{V_{in}} \tag{11}$$

$$P = \frac{p}{\rho V_{in}^2}, \theta = \frac{T - T_{in}}{T_h - T_{in}}, Re = \frac{2HV_{in}}{\nu_{nf}}, Pr = \frac{k_{nf}}{\rho_{nf} c_{p,nf}}$$

$$Ha = 2BH \sqrt{\frac{\sigma_{nf}}{\mu_{nf}}}, Gr = \frac{g \beta_{nf} (T_h - T_{in}) (2H)^3}{\nu_{nf}^2}$$

$$\frac{\partial U}{\partial X} + \frac{\partial V}{\partial Y} = 0 \tag{12}$$

$$\frac{\rho_{nf}}{\rho_{bf}} \left( U \frac{\partial U}{\partial X} + V \frac{\partial U}{\partial Y} \right) = -\frac{\partial P}{\partial X} + \frac{\mu_{nf}}{\mu_{bf}} \frac{1}{Re} \left( \frac{\partial^2 U}{\partial X^2} + \frac{\partial^2 U}{\partial Y^2} \right) \tag{13}$$

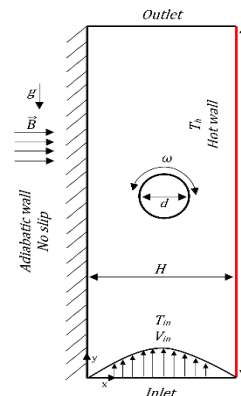


**Figure 1.** Schematic diagram of vertical channel with an inner rotating cylinder

**TABLE 1.** Thermophysical properties of water and Cu nanoparticles

	$\rho(\frac{kg}{m^3})$	$c_p(\frac{J}{kgK})$	$k(\frac{W}{mK})$	$\sigma(\frac{1}{\Omega.m})$	$\beta(\frac{1}{K})$
Water	996	4178	0.615	0.05	$2.94 \times 10^{-4}$
Copper	8933	385	401	$5.96 \times 10^7$	$1.67 \times 10^{-5}$

$$\frac{\rho_{nf}}{\rho_{bf}} (U \frac{\partial V}{\partial X} + V \frac{\partial V}{\partial Y}) = -\frac{\partial P}{\partial Y} + \frac{\mu_{nf}}{\mu_{bf}} \frac{1}{Re} \left( \frac{\partial^2 V}{\partial X^2} + \frac{\partial^2 V}{\partial Y^2} \right) - \frac{\sigma_{nf}}{\sigma_{bf}} \frac{Ha^2}{Re} V + \frac{\beta_{nf}}{\beta_{bf}} \frac{Gr}{Re^2} \theta \quad (14)$$

$$\frac{(\rho c_p)_{nf}}{(\rho c_p)_{bf}} (U \frac{\partial \theta}{\partial X} + V \frac{\partial \theta}{\partial Y}) = \frac{k_{nf}}{k_{bf}} \frac{1}{Re Pr} \left( \frac{\partial^2 \theta}{\partial X^2} + \frac{\partial^2 \theta}{\partial Y^2} \right) \quad (15)$$

**2. 2. Boundary Conditions** Non-dimensional boundary conditions of the channel with an inner rotating cylinder are:

Left wall:

$$U = V = 0, \frac{\partial \theta}{\partial X} = 0 \quad \& \quad \text{Right wall: } U = V = 0, \theta = 1$$

Inlet condition:  $U = 0, V = 1, \theta = 0$

$$\text{Cylinder: } \omega = \Omega, \frac{\partial \theta}{\partial \eta} = 0$$

where  $\eta$  is the normal vector to the surface and non-dimensional rotational speed of the cylinder can be

$$\text{obtained from: } \Omega = \frac{\omega d}{2V_{in}}$$

Local Nusselt number along the vertical hot wall of the channel is:

$$Nu_{local} = \frac{-k_{nf}}{k_f} \frac{\frac{\partial \theta}{\partial x}}{(1 - \theta_p)} \quad (16)$$

Furthermore, by integrating the local Nusselt number along the hot wall, the average Nusselt number can be expressed as:

$$Nu_{avg} = \frac{2H}{L} \int_0^{\frac{2H}{L}} Nu_{local} dY \quad (17)$$

Lift and Drag coefficients over the cylinder due to the Magnus and the flow separation effects are respectively presented as follows:

$$C_L = \frac{2F_{lift}}{\rho_{nf} V_{in}^2 d} \quad (18)$$

$$C_D = \frac{2F_{drag}}{\rho_{nf} V_{in}^2 d} \quad (19)$$

### 3. NUMERICAL PROCEDURE

Non-dimensional governing Equations 12-15 along with the corresponding non-dimensional boundary conditions are solved by using the Galerkin finite element method. Modification of the computed field variables and leading the residual to be zero over the computational domain is accomplished by using weighted functions.

$$\int_{\Omega} w f(x) R d\omega = 0 \quad (20)$$

where  $w, f, R, \omega$  and  $\Omega$  are weight function, residual, location variables and entire domain, respectively. Using weighted residual scheme, governing PDEs are simplified to integral equations, which are then solved in a matrix by the Newton-Raphson iteration method. The relative error for each field variable ( $\Gamma$ ) should satisfy:

$$\left| \frac{\Gamma^{n+1} - \Gamma^n}{\Gamma^{n+1}} \right| < 10^{-5} \quad (21)$$

where  $n$  represents the iteration number. The velocity components and pressure are discretized by utilizing P2-P1 Lagrange finite elements. In addition, Lagrange quadratic finite element was used to discretize temperature. Unstructured triangular grids are employed to the domain, which consisted higher resolution near the walls and the cylinder to augment precision at positions of higher gradients.

**3. 1. Validation** To ensure the accuracy of the numerical solution, the problem of Park et al. [34] is modeled to validate the present code results.

Figures 2 and 3 demonstrate the comparison of the streamlines and the isotherm contours versus different Rayleigh numbers for the present work and those of Park et al. [34] Furthermore, Figure 4 illustrates the Nusselt number variation along the walls of the cavity at  $Ra=10^3$ . According to these figures, the results of the present computational code are precise enough and are in excellent agreement with those of [34].

**3. 2. Grid Independency** In this study, to find out the solution mesh independency, the domain discretized to various numbers of elements. Figure 5 demonstrates the average Nusselt number in terms of element numbers of 2090, 4608, 7434, 11372, 52032 and 195692. According to this figure, by considering finer elements, results converge to a specific value and do not change significantly by increasing the numbers of

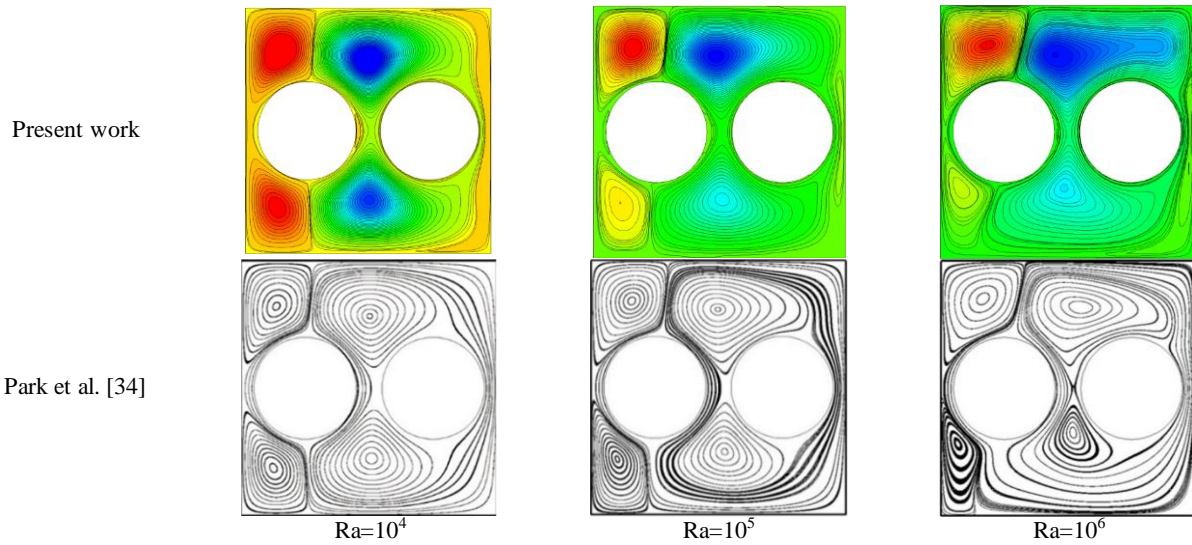


**Figure 2.** Comparison of streamlines for present work and that of Park et al. [34] in a square cavity with hot and cold inner stationary cylinder for different range of Rayleigh numbers

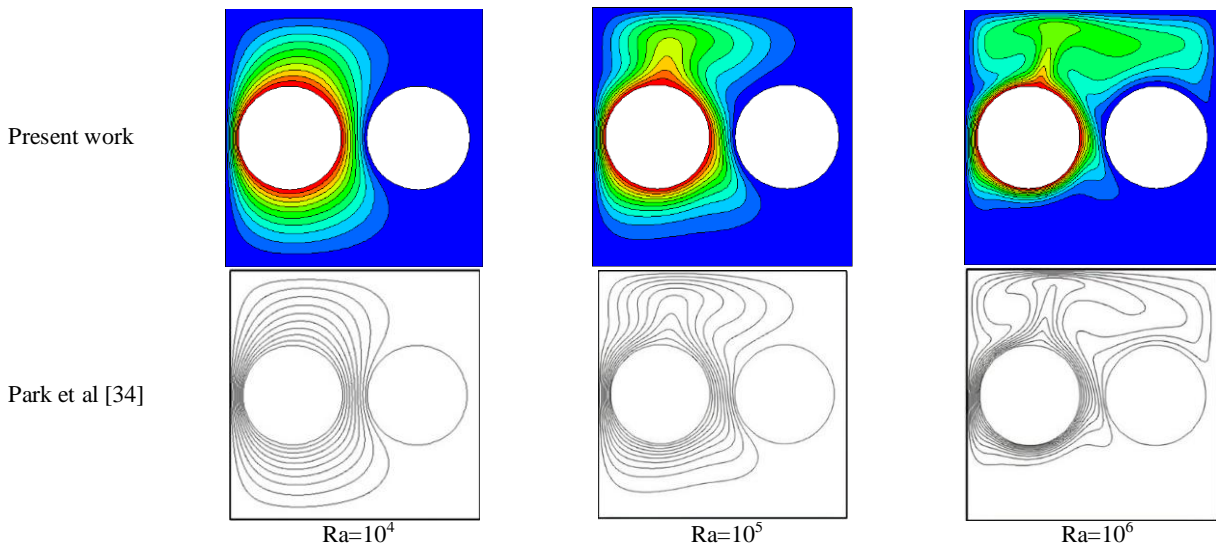


**Figure 3.** Isotherm contours comparison in square cavity with cold and hot inner stationary cylinder with present work and Park et al. [34] versus varying Rayleigh numbers

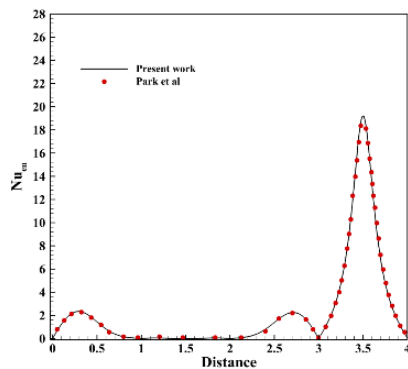


**Figure 4.** Comparison of the Nusselt number between present work and Park et al. [34] at  $Ra=10^3$

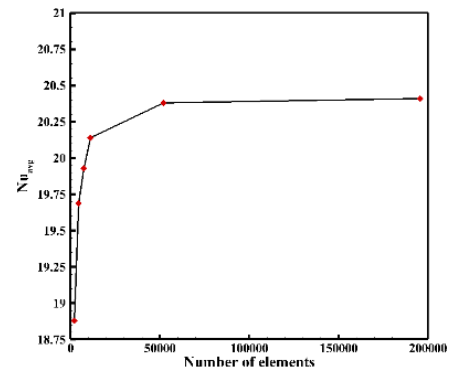


**Figure 5.** Average Nusselt number versus elements number for  $Ha = 60$  and  $\Omega = -10$

elements. As the figure shows, the average difference between Nusselt numbers for 52032 and 195692 grids is less than 0.15%. Thus, the 52032 grid is used in the rest of the simulations.

#### 4. RESULTS AND DISCUSSION

The study aims to investigate the effects of Hartmann number ( $0 \leq Ha \leq 60$ ) and non-dimensional angular velocity of the cylinder ( $-10 \leq \Omega \leq 10$ ) on the fluid flow and heat transfer in the channel. Simulation results are carried out for constant parameters of  $Re = 200$ ,  $\phi = 0.04$  for all cases.

##### 4. 1. Effects of Hartmann Number

Figure 6 illustrates the effects of different Hartmann numbers on the flow structure and isotherm contours. Constant parameters of  $\Omega = 3$  and varying  $Ha = 0, 20, 40, 60$  are considered for these simulations. As the streamlines show, in the case of no magnetic field ( $Ha = 0$ ), a large vortex is formed before the outlet on the hot wall. This vortex is formed because the separation occurs after the cylinder. As it can be observed, by raising the Hartmann number, due to the flow momentum reduction, the flow structure changes to a uniform configuration and the vortices eliminate disappear. In addition, there are two stagnation points in the flow field. The first stagnation point is at front of the cylinder and the second one is located at the left side of the cylinder, due to the counterclock-wise rotation of the cylinder. It can be seen, by augmenting the Hartmann number that locations of the stagnation points change and move toward the centerline of the channel. Despite the flow around the cylinder, the flow far away from the cylinder is not affected by the cylinder rotation in the higher Hartmann numbers. As evident from Figure 6, the cylinder rotation in the center of the channel causes to temperature boundary layer clings to the hot wall and consequently accelerate the convection heat transfer. As it is obvious from streamlines, the cylinder counterclockwise rotation conducts fluid flow from the hot wall to the adiabatic wall and leads to temperature layer thickness increment. Furthermore, at the front of the cylinder, the isotherms are squeezed gradually toward the hot wall by augmenting the Hartmann number. Similarly, the Lorentz force suppress the vorticities behind the cylinder, with this in mind that the size of the recirculation zones restrain as the Hartmann number increase.

Effects of the Hartmann number on the velocity profile at  $y/L=0.125$  are depicted in Figure 7. As the figure shows, the Hartmann number increment results in flatterting of the velocity profile at the mid-section of the channel, and accordingly, the velocity gradient adjust the walls increases. Similar conclusions have been reported in previous works as well. [20-21, 23, 25]

Figure 8 reveals the effects of Hartmann number variation on the local Nusselt number. As this figure shows, at the entry region of flow, by raising the Hartmann number, the local Nusselt number increment. This is due to the velocity increment at the vicinity of walls, resulting in improvement in the convective heat transfer.

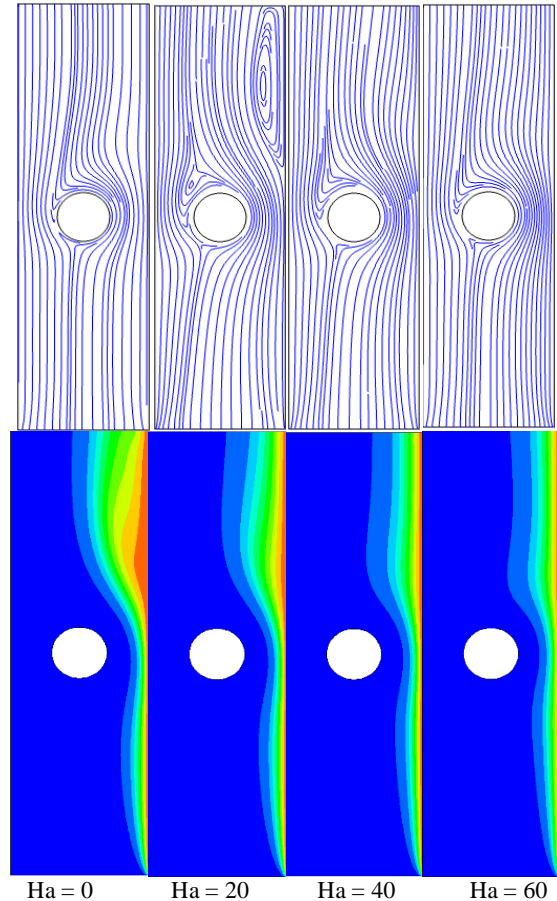


Figure 6. Streamlines and isotherm contours for numerous values of Hartmann number for  $\Omega = 3$

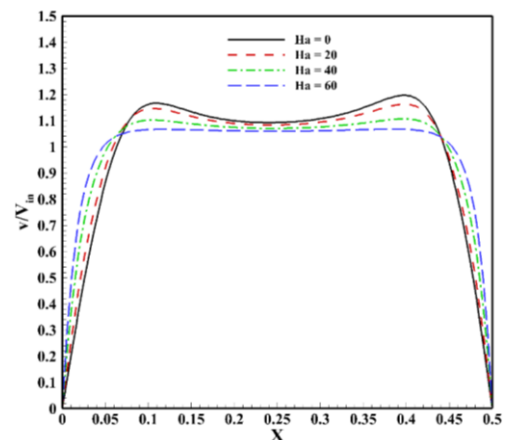
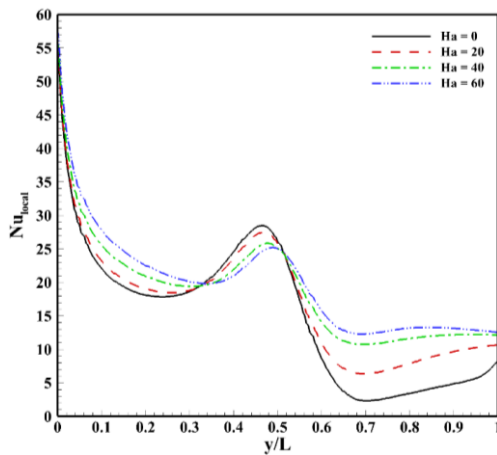


Figure 7. Influences of the Hartmann number on velocity profile at  $Y = 0.125$  for  $\Omega = 3$



**Figure 8.** Local Nusselt number variation along the hot wall against varying Hartmann number for  $\Omega = 3$

However, at the location of the cylinder, the flow structure is in the opposite of the entrance region. In where, the flow section area is smaller which leads to higher velocity on the hot wall and applying the magnetic field causes to reduce the velocity so as the Nusselt number. Furthermore, as shown in Figure 7, at the back of the cylinder, further raising in Hartmann number yields in local Nusselt number enhancement. This phenomenon corresponds to suppression of the vortices

by increasing Hartmann number that leads to improve convection heat transfer efficiency.

**4. 2. Effects of Non-dimensional Angular Velocity of the Cylinder**

Figure 9 demonstrates the effects of the cylinder rotation on the structure of flow and the isotherm contours for different non-dimensional angular velocity. Positive and negative values of  $\Omega$  represent counterclockwise and clockwise rotation of cylinder, respectively. As shown by streamlines, in the case of  $\Omega = 0$ , there is one stagnation point at the channel which takes place in front of the cylinder. This point appears when free stream encounters the cylinder. In addition, by enhancing non-dimensional velocity, second stagnation point appears at the left of the cylinder due to the counterclockwise rotation of the cylinder. Nonetheless, the density of the streamlines at the right side of the cylinder increases as the non-dimensional angular velocity increases, and hence the local velocity at this region rises. Furthermore, in the cases of CCW, the cylinder rotation diverts fluid flow from the hot wall to the adiabatic wall, which causes a recirculation zone to form behind the cylinder. In the cases of CW, however, the aforementioned influences are in opposite with CCW cases. According to the isotherms, in the direction of CCW, at the location of the cylinder, the cylinder rotation pushes isotherms to the hot wall which leads to a thin

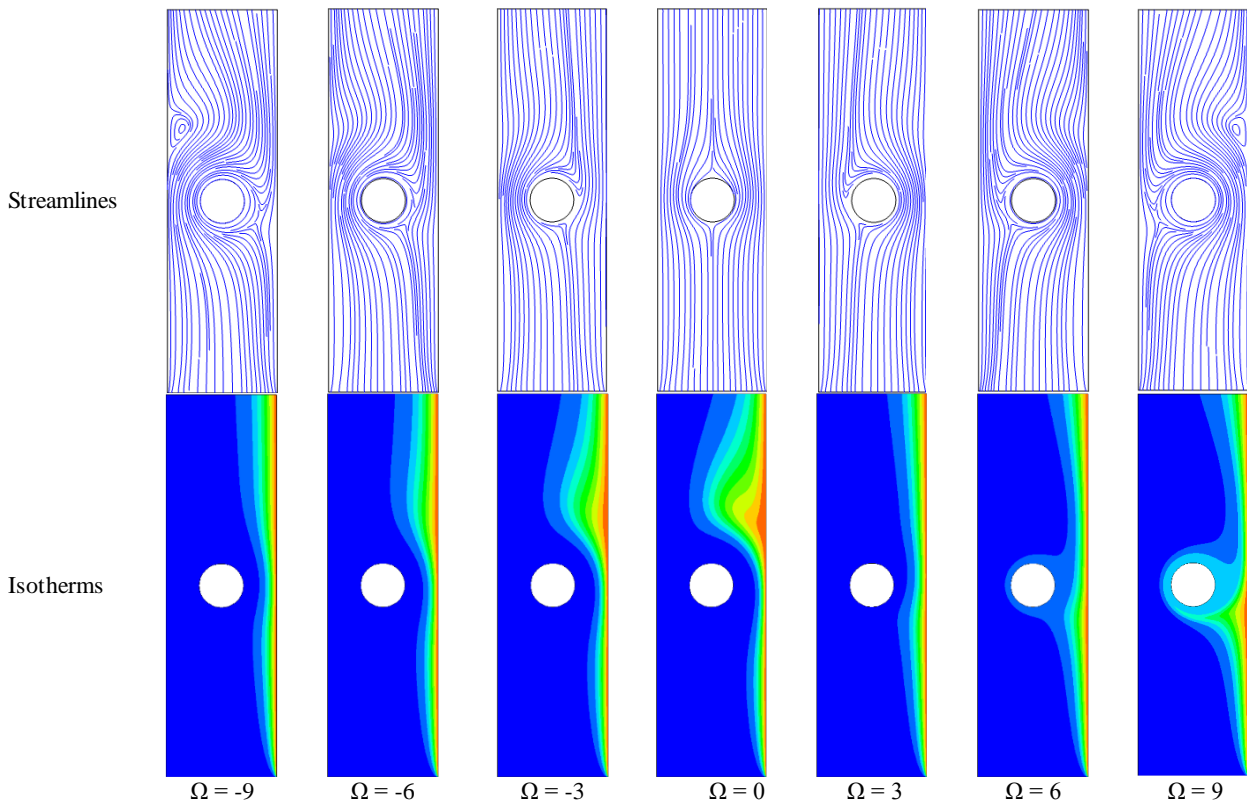


**Figure 9.** Impacts of the cylinder rotation on streamlines and isotherm contours for  $Ha = 30$

temperature layer. In addition, as mentioned in the previous section, the cylinder rotation forms a vortex behind the cylinder and this phenomenon widens the isotherms behind the cylinder.

However, in the cases of CW rotation of the cylinder, due to the streamlines, the net effect of the inlet velocity and the cylinder rotation causes the creation of a stagnation point before the cylinder. Therefore, the dominant heat transfer mechanism in this region is conduction. Moreover, due to the streamline compression after the cylinder on the hot wall, thickness of the isothermal lines decrease and therefore the convective heat transfer mechanism share increases.

The variations of the local Nusselt number alongside the hot wall with respect to the effects of counterclockwise rotation of the cylinder are demonstrated in Figure 10. As the results show, before the cylinder, any increment in  $\Omega$  has positive effects on the Nusselt number. It is due to the rotational velocity increment of the cylinder that pushes fluid flow to the hot wall and reduces the thermal boundary layer thickness. Oppositely, at the behind of the cylinder due to vortex generation on the hot wall, raising  $\Omega$  leads to reduce local Nusselt number.

Influences of the clockwise rotation of the cylinder on the local Nusselt number are illustrated in Figure 11. According to this figure, at the front of the cylinder, increment in angular velocity yields to the Nusselt number reduction. Because the net fluid flow velocity decreases by raising angular velocity that causes to thicken the thermal boundary layer. In contrast to the front region, at the back of the cylinder, increment in angular velocity has positive effects on the Nusselt number. The reason for the mentioned influence is related to pushing fluid flow to the hot wall by the cylinder which makes the thermal boundary layer thin and increases convective heat transfer.

Figure 12 represents the effect of  $\Omega$  on the average Nusselt number for different Hartmann numbers. As this figure depicts, in the condition of no magnetic field ( $Ha = 0$ ), in the ranges of  $-2 \leq \Omega \leq 0$  and  $0 < \Omega \leq 3$ , any change in the rotational speed of the cylinder has negative impact on the average Nusselt number. Additionally, in higher values of  $\Omega$ , due to the thermal boundary layer thickness reduction in the back of the cylinder, the average Nusselt number for both cases of CCW and CC rotations enhances. Furthermore, as the magnetic field augments, the effects of  $\Omega$  on the average Nusselt number is insignificant. For instance, at  $Ha = 45$  and  $60$ , the effects of  $\Omega$  on the average Nusselt number have almost been eliminated and its variations are independent of  $\Omega$ .

**4. 3. Lift and Drag Coefficients**

The effects of the non-dimensional angular velocity with varying Hartmann number on the lift coefficient are shown in

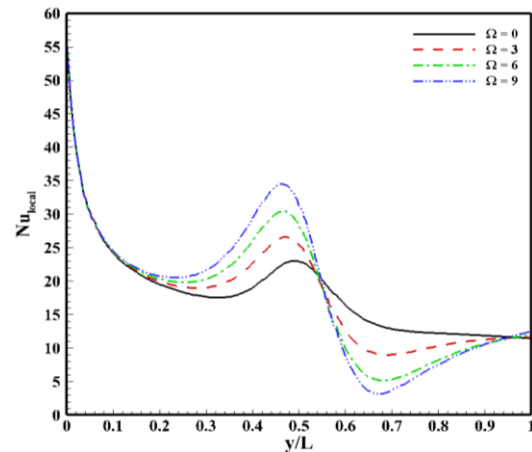


**Figure 10.** Effects of non-dimensional angular velocity of the cylinder in direction of counterclockwise rotation on the local Nusselt number for  $Ha = 30$

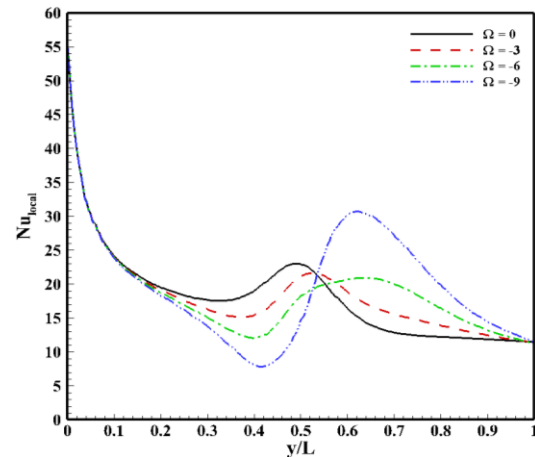


**Figure 11.** Variation of non-dimensional angular velocity of the cylinder in direction of clockwise rotation with the local Nusselt number for  $Ha = 30$

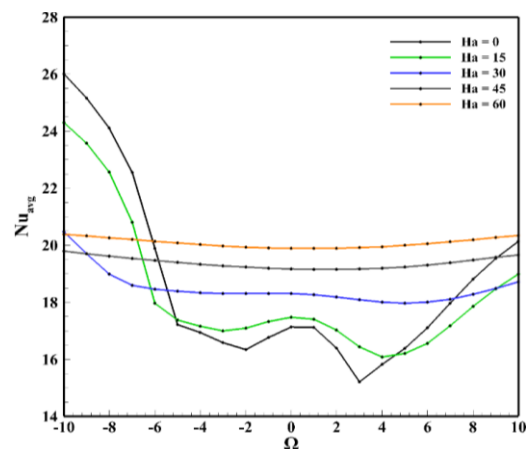


**Figure 12.** Average Nusselt number variation versus the cylinder rotation against various Hartmann numbers

Figure 13. As this figure illustrates, any increase in  $\Omega$  in terms of CCW and CW rotations of the cylinder causes to decrease and increase lift coefficient, respectively. In contrast to CW rotation, as  $\Omega$  rises in CCW direction, the flow at the right side of the cylinder accelerates which forces the pressure gradient to lower and consequently, the lift force becomes higher. Moreover, as the magnetic field strength increases, the magnitude of  $C_L$  at both rotation directions decrease. This phenomenon corresponds to the momentum reduction due to the higher Hartmann number that leads to a decrease in lift force. Moreover, the negative values of the lift coefficient represent the opposite direction of the lift force. Additionally, it is worth to mention that, the value of the lift coefficient at stationary case of the cylinder ( $\Omega = 0$ ) is zero and does not changes with the Hartmann number. It is due to symmetric fluid flowing on the stationary cylinder.

Figure 14 demonstrates the effect of varying  $\Omega$  on the drag coefficient for different Hartmann numbers. As shown in this figure, in the case of no magnetic field ( $Ha = 0$ ), any enhancement in  $\Omega$  magnitude, in turn, increases the drag coefficient. Moreover, by increasing  $\Omega$ , the rotational cylinder causes to guide the flow to the back of the cylinder that leads to creating a negative pressure gradient and therefore the drag force increases. Similarly, as the magnetic field is increased, for lower numbers of  $\Omega$  ( $-5 \leq \Omega \leq 5$ ) drag coefficient increases. It is worth to say that applying the magnetic field eliminates wake regions behind the cylinder. As Figure 14 shows, any increment in the Hartmann number results in a uniform distribution of the drag coefficient. In other words, the Hartmann number decreases the dependence of the drag coefficient on non-dimensional velocity. This phenomenon is due to the braking action of the Lorentz force that controls fluid flow and restrains fluctuations.

## 5. CONCLUSION

Heat transfer and fluid flow of the straight vertical channel with adiabatic rotating cylinder utilizing nanofluid affected by uniform magnetic field are numerically studied. Effective parameters such as Hartmann number and direction of rotation are examined. Following points can be concluded from this study:

- Magnetic field reduces the velocity of the core flow while it increases the velocity near walls, and therefore enhances the convection heat transfer.
- In absence of the magnetic field, the cylinder rotation causes vortex to form behind the cylinder near the walls. However, by applying magnetic field the vortex weakens.
- The highest Nusselt numbers achieved at  $\Omega = -10$  in the case of no magnetic field and enhancement due to the motionless cylinder is 51%.
- In higher Hartmann numbers, the average Nusselt number does not change remarkably with  $\Omega$ .
- Magnitude of the drag and the lift coefficients of the cylinder increased in higher  $\Omega$ s. In addition, applying the magnetic field leads to a decrease in lift coefficient and reduces the dependency of the drag coefficient to  $\Omega$ .

## 5. REFERENCES

1. Ganvir, R., P. Walke, and V. Kriplani, "Heat transfer characteristics in nanofluid—a review", *Renewable and Sustainable Energy Reviews*, Vol. 75, (2017), 451-460, <https://doi.org/10.1016/j.rser.2016.11.010>
2. Hussein, A.M., K. Sharma, R. Bakar, and K. Kadrigama, "A review of forced convection heat transfer enhancement and hydrodynamic characteristics of a nanofluid", *Renewable and Sustainable Energy Reviews*, Vol. 29, (2014), 734-743, <https://doi.org/10.1016/j.rser.2013.08.014>
3. Kakaç, S. and A. Pramuanjaroenkij, "Review of convective heat transfer enhancement with nanofluids", *International Journal of Heat and Mass Transfer*, Vol. 52, (2009), 3187-3196, <https://doi.org/10.1016/j.ijheatmasstransfer.2009.02.006>
4. Li, Y., S. Tung, E. Schneider, and S. Xi, "A review on development of nanofluid preparation and characterization", *Powder Technology*, Vol. 196, (2009), 89-101, <https://doi.org/10.1016/j.powtec.2009.07.025>
5. Tawfik, M.M., "Experimental studies of nanofluid thermal conductivity enhancement and applications: a review", *Renewable and Sustainable Energy Reviews*, Vol. 75, (2017), 1239-1253, <https://doi.org/10.1016/j.rser.2016.11.111>
6. Yu, W., D.M. France, J.L. Routbort, and S.U. Choi, "Review and comparison of nanofluid thermal conductivity and heat transfer enhancements", *Heat Transfer Engineering*, Vol. 29, (2008), 432-460, <https://doi.org/10.1080/01457630701850851>
7. Gravndyan, Q., O.A. Akbari, D. Toghraie, A. Marzban, R. Mashayekhi, R. Karimi, and F. Pourfattah, "The effect of aspect ratios of rib on the heat transfer and laminar water/TiO<sub>2</sub> nanofluid flow in a two-dimensional rectangular microchannel", *Journal of Molecular Liquids*, Vol. 236, (2017), 254-265, <https://doi.org/10.1016/j.molliq.2017.04.030>
8. Ahmadi, A.A., E. Khodabandeh, H. Moghadasi, N. Malekian, O.A. Akbari, and M. Bahiraei, "Numerical study of flow and heat transfer of water-Al<sub>2</sub>O<sub>3</sub> nanofluid inside a channel with an inner cylinder using Eulerian-Lagrangian approach", *Journal of Thermal Analysis and Calorimetry*, Vol. 132, (2018), 651-665, <https://doi.org/10.1007/s10973-017-6798-y>
9. Bahiraei, M. and P.R. Mashaie, "Using nanofluid as a smart suspension in cooling channels with discrete heat sources", *Journal of Thermal Analysis and Calorimetry*, Vol. 119, (2015), 2079-2091, <https://doi.org/10.1007/s10973-015-4414-6>
10. Ho, C.-J., L. Wei, and Z. Li, "An experimental investigation of forced convective cooling performance of a microchannel heat sink with Al<sub>2</sub>O<sub>3</sub>/water nanofluid", *Applied Thermal Engineering*, Vol. 30, (2010), 96-103, <https://doi.org/10.1016/j.applthermaleng.2009.07.003>
11. Heidary, H. and M. Kermani, "Heat transfer enhancement in a channel with block (s) effect and utilizing Nano-fluid", *International Journal of Thermal Sciences*, Vol. 57, (2012), 163-171, <https://doi.org/10.1016/j.ijthermalsci.2012.02.001>
12. Khanafer, K., K. Vafai, and M. Lightstone, "Buoyancy-driven heat transfer enhancement in a two-dimensional enclosure utilizing nanofluids", *International Journal of Heat and Mass*

- Transfer*, Vol. 46, (2003), 3639-3653, [https://doi.org/10.1016/S0017-9310\(03\)00156-X](https://doi.org/10.1016/S0017-9310(03)00156-X)
13. Santra, A.K., S. Sen, and N. Chakraborty, "Study of heat transfer due to laminar flow of copper-water nanofluid through two isothermally heated parallel plates", *International Journal of Thermal Sciences*, Vol. 48, (2009), 391-400, <https://doi.org/10.1016/j.ijthermalsci.2008.10.004>
  14. Roslan, R., H. Saleh, and I. Hashim, "Effect of rotating cylinder on heat transfer in a square enclosure filled with nanofluids", *International Journal of Heat and Mass Transfer*, Vol. 55, (2012), 7247-7256, <https://doi.org/10.1016/j.ijheatmasstransfer.2012.07.051>
  15. Chen, C.-H., "Heat and mass transfer in MHD flow by natural convection from a permeable, inclined surface with variable wall temperature and concentration", *Acta Mechanica*, Vol. 172, (2004), 219-235, <https://doi.org/10.5281/zenodo.1091654>
  16. Daniel, Y.S., Z.A. Aziz, Z. Ismail, and F. Salah, "Effects of thermal radiation, viscous and Joule heating on electrical MHD nanofluid with double stratification", *Chinese Journal of Physics*, Vol. 55, (2017), 630-651, <https://doi.org/10.1016/j.cjph.2017.04.001>
  17. Ma, Y., R. Mohebbi, M. Rashidi, Z. Yang, and M.A. Sheremet, "Numerical study of MHD nanofluid natural convection in a baffled U-shaped enclosure", *International Journal of Heat and Mass Transfer*, Vol. 130, (2019), 123-134, <https://doi.org/10.1016/j.ijheatmasstransfer.2018.10.072>
  18. Mabood, F. and W. Khan, "Analytical study for unsteady nanofluid MHD Flow impinging on heated stretching sheet", *Journal of Molecular Liquids*, Vol. 219, (2016), 216-223, <https://doi.org/10.1016/j.molliq.2016.02.071>
  19. Makinde, O. and I. Animasaun, "Bioconvection in MHD nanofluid flow with nonlinear thermal radiation and quartic autocatalysis chemical reaction past an upper surface of a paraboloid of revolution", *International Journal of Thermal Sciences*, Vol. 109, (2016), 159-171, <https://doi.org/10.1016/j.ijthermalsci.2016.06.003>
  20. Aminossadati, S., A. Raisi, and B. Ghasemi, "Effects of magnetic field on nanofluid forced convection in a partially heated microchannel", *International Journal of Non-Linear Mechanics*, Vol. 46, (2011), 1373-1382, <https://doi.org/10.1016/j.ijnonlinmec.2011.07.013>
  21. Heidary, H., R. Hosseini, M. Pirmohammadi, and M. Kermani, "Numerical study of magnetic field effect on nano-fluid forced convection in a channel", *Journal of Magnetism and Magnetic Materials*, Vol. 374, (2015), 11-17, <https://doi.org/10.1016/j.jmmm.2014.08.001>
  22. Selimefendigil, F. and H.F. Öztop, "Numerical study of MHD mixed convection in a nanofluid filled lid driven square enclosure with a rotating cylinder", *International Journal of Heat and Mass Transfer*, Vol. 78, (2014), 741-754, <https://doi.org/10.1016/j.ijheatmasstransfer.2014.07.031>
  23. Hosseini, S., M. Sheikholeslami, M. Ghasemian, and D. Ganji, "Nanofluid heat transfer analysis in a microchannel heat sink (MCHS) under the effect of magnetic field by means of KKL model", *Powder Technology*, Vol. 324, (2018), 36-47, <https://doi.org/10.1016/j.powtec.2017.10.043>
  24. Oztop, H.F., K. Al-Salem, and I. Pop, "MHD mixed convection in a lid-driven cavity with corner heater", *International Journal of Heat and Mass Transfer*, Vol. 54, (2011), 3494-3504, <https://doi.org/10.1016/j.ijheatmasstransfer.2011.03.036>
  25. Aminfar, H., M. Mohammadpourfard, and F. Mohseni, "Two-phase mixture model simulation of the hydro-thermal behavior of an electrical conductive ferrofluid in the presence of magnetic fields", *Journal of Magnetism and Magnetic Materials*, Vol. 324, (2012), 830-842, <https://doi.org/10.1016/j.jmmm.2011.09.028>
  26. Ma, Y., R. Mohebbi, M. Rashidi, and Z. Yang, "MHD convective heat transfer of Ag-MgO/water hybrid nanofluid in a channel with active heaters and coolers", *International Journal of Heat and Mass Transfer*, Vol. 137, (2019), 714-726, <https://doi.org/10.1016/j.ijheatmasstransfer.2019.03.169>
  27. Mahmoudi, A.H., I. Pop, and M. Shahi, "Effect of magnetic field on natural convection in a triangular enclosure filled with nanofluid", *International Journal of Thermal Sciences*, Vol. 59, (2012), 126-140, <https://doi.org/10.1016/j.ijthermalsci.2012.04.006>
  28. Bianco, V., F. Chiacchio, O. Manca, and S. Nardini, "Numerical investigation of nanofluids forced convection in circular tubes", *Applied Thermal Engineering*, Vol. 29, (2009), 3632-3642, <https://doi.org/10.1016/j.applthermaleng.2009.06.019>
  29. Garoosi, F., F. Hoseinnejad, and M.M. Rashidi, "Numerical study of natural convection heat transfer in a heat exchanger filled with nanofluids", *Energy*, Vol. 109, (2016), 664-678, <https://doi.org/10.1016/j.energy.2016.05.051>
  30. Pak, B.C. and Y.I. Cho, "Hydrodynamic and heat transfer study of dispersed fluids with submicron metallic oxide particles", *Experimental Heat Transfer an International Journal*, Vol. 11, (1998), 151-170, <https://doi.org/10.1080/08916159808946559>
  31. Brinkman, H., "The viscosity of concentrated suspensions and solutions", *The Journal of Chemical Physics*, Vol. 20, (1952), 571-571, <https://doi.org/10.1063/1.1700493>
  32. Wasp, E.J., J.P. Kenny, and R.L. Gandhi, "Solid-liquid flow: slurry pipeline transportation. [Pumps, valves, mechanical equipment, economics]", Ser. Bulk Mater. Handl.; (United States), Vol. 1, (1977), <https://www.osti.gov/biblio/6343851>
  33. Maxwell, J.C., A treatise on electricity and magnetism. Vol. 1. 1873: Oxford: Clarendon Press.
  34. Park, Y.G., H.S. Yoon, and M.Y. Ha, "Natural convection in square enclosure with hot and cold cylinders at different vertical locations", *International Journal of Heat and Mass Transfer*, Vol. 55, (2012), 7911-7925, <https://doi.org/10.1016/j.ijheatmasstransfer.2012.08.012>

---

### Persian Abstract

#### چکیده

امروزه تحلیل انتقال حرارت در کانال‌ها و محفظه‌ها مورد توجه بسیاری از پژوهش‌گران قرار گرفته است. در کار حاضر جریان و انتقال حرارت نانوسیال در یک کانال عمودی که شامل یک استوانه‌ی چرخان می‌باشد، به صورت عددی مطالعه گردیده است. میدان مغناطیسی یک‌نواخت به سیال اعمال شده و تاثیر جهت‌های مختلف چرخش استوانه □ عدد هارتمن و سرعت دورانی استوانه بررسی شده است. نتایج نشان می‌دهد که با افزایش عدد هارتمن □ در سرعت‌های دورانی کم استوانه □ عدد ناسلت متوسط افزایش می‌یابد. برخلاف آن □ در اعداد هارتمن بالاتر □ عدد ناسلت متوسط تغییرات چشمگیری با سرعت زاویه‌ای بی‌بعد ندارد. علاوه بر آن □ مطالعه‌ی ضرایب درگ و برآ نشان می‌دهد که در عدد هارتمن ثابت □ بیشترین ضریب درگ در بیشترین سرعت زاویه‌ای استوانه اتفاق می‌افتد. به همین ترتیب □ توزیع تقریباً یک‌نواخت ضریب درگ در اعداد هارتمن بزرگتر مشاهده می‌شود. نتایج عددی با گزارش‌های گذشته مقایسه شده و این مقایسه تطابق بسیار مناسب بین آنها را نشان می‌دهد.